Impact pressure on an orifice plate by a rising water column driven by an air pocket in a vertical riser

Yu Qian and David Z. Zhu

ABSTRACT

Occurrences of storm geyser events have attracted significant attention in recent years. Previous studies suggest that using an orifice plate can reduce the intensity of a geyser event but may induce a water-hammer type of pressure on the orifice plate. This study was conducted to explore the factors that influence the pressure transients when an orifice plate was installed in a vertical riser. A novel model was developed to simulated the movement of a rising water column driven by an air pocket in a vertical riser with an orifice plate on the top. Water-hammer type of pressure occurs when the water column reaches the orifice plate. The current model accurately simulates the dynamics of the water column considering its mass loss due to the flow along the wall of the riser (film flow) and the existence of the orifice plate. It was found that the initial water column length and the driving pressure, as well as the riser material, have a strong relationship with the peak pressure. The riser diameter and riser height have minor effect on the peak pressure. The water-hammer induced peak pressure reaches the maximum when the orifice opening is around 0.2 times the diameter of the vertical riser.

Key words | air–water flow, numerical method, orifice plate, storm geyser, water hammer

Yu Qian
Department of Civil and Environmental Engineering,
University of Alberta,
Edmonton, AB T6G 2W2,
Canada

David Z. Zhu (corresponding author)
Department of Civil and Environmental Engineering,
University of Alberta,
Edmonton, AB T6G 2W2,
Canada
and
School of Civil and Environmental Engineering,
Ningbo University,
Zhejiang,
China
E-mail: *david.zhu@ualberta.ca*

INTRODUCTION

Geyser events in storm sewer systems are commonly seen as the eruptions of air/water mixture out of manholes, and have attracted significant attention in recent decades due to public safety issues (Li & McCorquodale 1999; Shao 2013). Recently a few studies reported that an orifice plate installed in the manhole (or riser) is able to reduce the total volume of water flowing out of the riser during geyser events, but it might induce a water-hammer type of pressure (Huang *et al.* 2018a, 2018b; Qian *et al.* 2020). However, the factors affecting the dynamics of pressure were not discussed in detail. Therefore, there is urgent need to understand the detailed air–water processes related to the use of an orifice plate, in particular, the effect of orifice opening size and the physical properties of manhole on the pressure transient induced by geyser events.

The hydraulics of water flowing in and out of manholes without the interaction with air pockets were studied by Rubinato *et al.* (2018), and Beg *et al.* (2019), and Lopes *et al.* (2015). Hamam & McCorquodale (1982) summarized the processes of a rapid filling pipe, and proposed a rigid water column method for modeling the pressure transients. A series of studies on geysers in prototype sewer systems were done by Wright *et al.* (2008, 2011a, 2011b), Vasconcelos & Wright (2009) and Lewis (2011). The mechanism of geyser events was proposed as the release of pressurized air pockets with water remaining in the riser. Considering the mass loss due to the water flow along the wall of the riser, which is named film flow, the movement of the water column pushed by an air pocket in the riser was studied in Vasconcelos & Wright (2011). Cong *et al.* (2017) and Liu *et al.* (2020) experimentally studied the mechanisms of storm geysers and the pressure transient during geyser events in laboratory scale.

For computational fluid dynamic (CFD) models, Zhou *et al.* (2011) developed a two-dimensional CFD model simulating the releasing of an air pocket in a hypothetical pipe. It was found that the maximum impinging pressure occurs when the orifice opening is about 0.2 times the pipe diameter. Chan *et al.* (2018) simulated the detailed flow pattern based on the study of Cong *et al.* (2017). Shao & Yost (2018) numerically investigated the geyser events at model scale. Qian *et al.* (2020) numerically assessed the effectiveness of different geyser

doi: 10.2166/wst.2020.191

mitigation methods. Huang *et al.* (2018a, 2018b) assessed the effectiveness of an orifice plate on mitigation of geyser events in a laboratory scale. The top of the riser for the above studies was fully open except for Qian *et al.* (2020) and Huang *et al.* (2018a, 2018b), who proposed an orifice plate as geyser mitigation method, but not many other studies were conducted on its further application.

For numerical and analytical efforts on storm geysers, a combined rigid column method and method of characteristics of solving the pressure change was proposed by Zhou *et al.* (2002, 2004). Following Zhou *et al.* (2002), Li & Zhu (2018) numerically simulated the pressure change due to rapid filling in a horizontal pipe with an end orifice. These studies focus on the release of the air pocket via the orifice plate in a horizontal pipe driven by a water column connected to a constant pressure water tank. In prototype storm sewer systems, a sandwich pattern of air and water may exist (Huang *et al.* 2018a) in the riser. For all above studies, the top of the shaft was also fully open except for Huang *et al.* (2018a). In prototype sewer systems, the manhole cover is usually smaller than the manhole (City of Edmonton 2015). Adding an orifice plate at the top of the riser in experiment design reflects the real case. Therefore, calculating the hydrodynamics of a moving water column driven by an air pocket as well as its interaction with an orifice at the top of a riser is of interest.

There are two major considerations for modeling storm geyser events: (1) the water column is driven by an air pocket and its length decreases due to the film flow; and (2) the riser is with an orifice plate on the top. This study was conducted to consider these points for the first time. A theoretical model was developed for calculating the movement of a water column in a riser pushed by an air pocket at the bottom. The model can be used to predict the pressure variation at the top of the riser induced by the impingement of water column. This study also examines the effect of the orifice opening size on the peak pressure value.

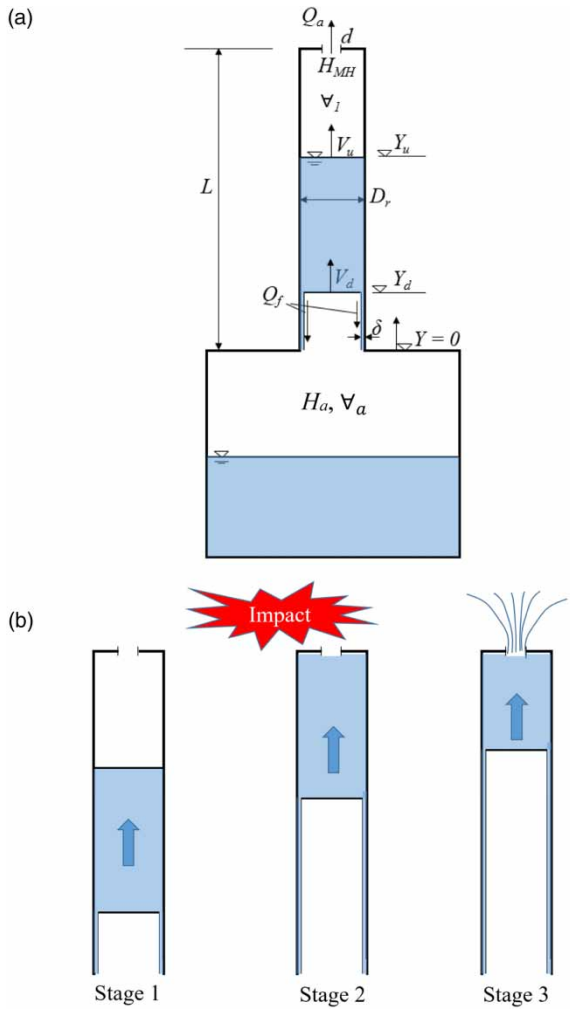

Figure 1 | Schematic of the model for theoretical calculation. (a): control volume of the model; (b): illustration of stages 1–3.

METHODOLOGY

Governing equations

A riser with a diameter of D_r and height of L is shown in Figure 1(a). A water column is predefined in the riser and the top and bottom position of the water column are denoted as Y_u and Y_d. The origin of Y is at the bottom of the riser. An air pocket with an initial volume of $\forall_0$ and initial pressure head of H_0 is defined below the water column, and an orifice with an opening diameter of d is defined at the top of the riser. By tracking the position of Y_u and Y_d, a theoretical model can be developed. During the process, before the water column impinges on the orifice plate, the length of the water column $(Y_u - Y_d)$ decreases due to the film flow around the riser.

The following assumptions are made in the model. Firstly, the air phase undergoes an isentropic expansion/compression process where the polytropic exponent $k = 1.4$ (Zhou *et al.* 2004). Secondly, the top and bottom of the water column are horizontal and the water column remains a single phase without air entrainment. This assumption is supported by the fact that the height of the riser is typically an order of magnitude (>10 times) larger than its diameter. Therefore, the asymmetry distribution of the water surface in the process can be ignored.

It is reasonable to estimate the water column volume decrease due to the film flow (Vasconcelos & Wright 2011), and the flow rate of the film flow (Q_f) and the thickness of the film flow (δ) can be written as:

$$Q_f = A' U_\infty \tag{1}$$

$$\frac{\pi}{4} U_\infty (D_r - 2\delta)^2 = \frac{\pi}{3} \frac{g D_r (\rho_w - \rho_a)\delta^3}{\mu_w} \tag{2}$$

where: U_∞ is the velocity of the Taylor bubble and it equals the velocity of the bottom of the water column at $t = 0$ s and $U_\infty = 0.345\sqrt{gD_r}$ (Vasconcelos & Wright 2011), ρ_w and ρ_a are water and air density respectively, A' is the cross-sectional area of the riser minus the space occupied by the film flow, μ_w is the dynamic viscosity of water. The thickness of the film flow is obtained by plotting Equation (2) for δ and D_r, which yields $\delta = 0.0045 D_r^{0.5269}$ with $R^2 = 0.99$.

Shown in Figure 1(b), the flow process can be divided into three stages. For Stage 1, the water column is pushed by the air pocket below it and moves upward. Once the top of the water column reaches the orifice plate, a water-hammer type pressure occurs and it is categorized as Stage 2. After the impingement, water continuously ejects from the orifice plate until it is fully discharged, which is defined as Stage 3. A detailed description is provided below.

Stage 1

Prior to the top of the water column (Y_u) reaching the orifice plate, Vasconcelos & Wright (2011) studied the movement of top and bottom of the water column. The governing equations for the water column and air phase below the water column can be written as:

$$\frac{dV_d}{dt} = \frac{g}{Y_u - Y_d}\left[\frac{Q_f V_d}{gA} + (H_a - H_{MH}) - (Y_u - Y_d) - f\frac{(Y_u - Y_d)}{D_r}\frac{|V_d|V_d}{2g}\right] \tag{3}$$

$$\frac{dY_d}{dt} = V_d \tag{4}$$

$$\frac{d\forall_a}{dt} = \frac{\pi}{4}(D_r - 2\delta)^2 V_d - Q_f \tag{5}$$

$$\frac{dH_a^*}{dt} = -\frac{kH_a^*}{\forall_a}\frac{d\forall_a}{dt} \tag{6}$$

$$\frac{dY_u}{dt} = -\frac{1}{A}\frac{d\forall_1}{dt} = -V_u \tag{7}$$

$$\frac{dV_u}{dt} = \frac{d\left(-\frac{1}{A}\frac{d\forall_1}{dt}\right)}{dt} = -\frac{(D_r - 2\delta)^2}{D_r^2}\frac{dV_d}{dt} \tag{8}$$

where: t is time, V_u, V_d are the velocity of the top and bottom of the water column, g is the acceleration due to gravity, A is the cross-sectional area of the riser, f is the wall friction coefficient, H_a and $\forall_a$ are the head and volume of the air pocket below the water column, respectively, H_{MH} and $\forall_1$ are the pressure head and volume of the air pocket above the water column, respectively. The asterisk denotes the absolute pressure head. In Equation (3), the velocity at the bottom of the water column in the riser is used to calculate the friction loss. This is because the friction coefficient is in the order of 0.02 or less, and the difference between the velocity of the top and bottom of the water column is relatively small.

At this stage, the air phase above the water column is controlled by the equations (Zhou *et al.* 2002):

$$\frac{d\forall_1}{dt} = -AV_u \tag{9}$$

$$\frac{dH_{MH}^*}{dt} = -k\frac{H_{MH}^*}{\forall_1}\left(\frac{d\forall_1}{dt} + Q_a\right) \tag{10}$$

where: Q_a is the air flow rate via orifice and can be written as:

$$Q_a = C_d A_0 M\sqrt{2g\frac{\rho_w}{\rho_a}H_{MH}} \tag{11}$$

and

$$M = \left[\frac{k}{k-1}\left(\frac{H_0}{H_{MH}^*}\right)^{2/k}\frac{1 - (H_0/H_{MH}^*)^{(k-1)/k}}{1 - H_0/H_{MH}^*}\right]^{1/2} \quad \text{for } H_{MH}^*/H_0 < 1.89 \tag{12}$$

$$M = \sqrt{\frac{1}{2}\left(\frac{H_{MH}^*}{H_{MH}}\right)}\sqrt{k\left(\frac{2}{k+1}\right)^{(k+1)/(k-1)}} \quad \text{for } H_{MH}^*/H_0 > 1.89 \tag{13}$$

where: C_d is a constant of 0.65, A_0 is the area of the orifice opening.

Stage 2

Once the water column reaches the orifice, Qian *et al.* (2020) suggested that a water-hammer type pressure occurs by the momentum change of the water column. A water-hammer type pressure can be written as:

$$\frac{dH_{MH}}{dt} = \frac{1}{\rho_w g}\left(-\rho_m c \frac{dV_u}{dt}\right) \tag{14}$$

where: ρ_m is the density of the air/water mixture, c is the pressure pulse wave speed and can be written as: $c = \sqrt{\frac{B/\rho_w}{1+(D_r/e)(B/E)}}$, where B is the bulk elastic modulus of water at 2.2 GPa (Potter *et al.* 2012), E is the elastic modulus of the pipe material, and e is the pipe wall thickness: 0.008 m in this study. The peak pressure generated by the water-hammer effect is denoted as H_{PK}. For a rigid pipe, the pressure wave speed can reach up to 1,485 m/s. The elasticity of pipe materials would alter the pressure wave speed and therefore change the pressure peak. In this study, both PVC and steel pipe materials are tested: $E_{PVC} =$ 4.7 GPa, and $E_{Steel} =$ 200 GPa.

Stage 3

After the impingement of water column on the orifice plate, the water flow rate through the orifice can be written as $A_0\sqrt{\frac{2gH_{MH}}{1+K}}$. Depending on the mass conservation, the velocity of the bottom of the water column can be written as:

$$V_d = \frac{A_0\sqrt{\frac{2gH_{MH}}{1+K}} + Q_f}{A} \tag{15}$$

in which K is the minor head loss due to the orifice plate.

Table 1 is a summary of all experimental conditions. The value of $(Y_{u0} - Y_{d0})$ represents the initial water column length. Run A and Run B are model calibration and validation with the experimental data from Liu (2018) and Vasconcelos & Wright (2011) for PVC risers. Run A also serves for testing the effect of driving pressure and initial water column length. Runs C and D are for testing the effect of the riser diameter and height of the riser for PVC risers. Run E is for testing the effect of a steel riser. A total of 201 runs were conducted. Each run contains 96 calculations where the orifice size ranged from $0.05D_r$ to $0.99D_r$.

Table 1 | List of experimental arrangements

Run	D_r (m)	L (m)	$(Y_{u0} - Y_{d0})/L$	d/D_r	H_0 (m)	$\forall_0$ (L)	Riser material
A	0.055	0.78	0.3, 0.39[a], 0.6, 0.8	0.05–0.99	1[a], 5, 10	71	PVC
B	0.013[b]	0.61	0.5, 0.75	0.99	0.305, 0.610	3.8	
C1	0.055	1.22	0.3, 0.5, 0.6, 0.8	0.05–0.99	1, 5, 10, 20	100	
C2	0.1						
C3	0.2						
C4	0.3						
D1	0.055	0.78	0.3, 0.5, 0.6, 0.8	0.05–0.99	1, 5, 10, 20	100	
D2		1.0					
D3		1.5					
D4		1.7					
D5		2.0					
E1	0.055	0.78	0.3, 0.5, 0.6, 0.8	0.05–0.99	1, 5, 10, 20	50	Steel
E2		1.5					
E3	0.1	1.5					
E4	0.3						

[a]Model calibration and validation at $d/D_r = 0.1$ and 0.5.
[b]Model validation with Vasconcelos & Wright (2011).

The governing equations listed above are solved numerically using a fourth-order Runge–Kutta algorithm. The calculation stops when the water column length decreases to zero.

Model calibration and validation

Data from the experiment conducted by Liu (2018) in PVC risers was used for model calibration and validation. The riser had a diameter of 0.06 m and length of 0.78 m. An orifice plate was installed at the top of the riser, and the orifice size was 0.1 and 0.5 times the riser diameter. The inflow rate was measured by a magnetic flow meter. Pressure was measured immediately below the orifice plate in the riser using a pressure sensor. A video camera was used to capture the geyser process at 120 fps. The detailed measurement setup can be found in Liu (2018). For model calibration and validation, H_0 was 1 m, and $\forall_0$ was 71 L.

For model calibration, the right hand of Equation (4) is to be multiplied by a factor of 1.15 to match the measured water column. This is mainly due to the film flow causing additional velocity at the bottom. The loss coefficient f follows the equation proposed by Arai & Yamamoto (2003):

$$f = \left[1.14 - 2\log_{10}\left(\frac{\varepsilon}{D_r} + \frac{21.25}{Re^{0.9}}\right)\right]^{-2} \tag{16}$$

where: $\frac{\varepsilon}{D_r}$ is the relative roughness of pipe materials, Re is Reynold's number of the water flow based on V_d and D_r.

The comparison of the calculated and measured Y_u and Y_d as well as the pressure under the orifice plate is plotted in Figure 2(a) and 2(b) for Run A for $d/D_r = 0.5$ and 0.1. The model results in a peak pressure of 6.75 m and 10.48 m respectively. Comparing with the measured 6.58 m and 10.49 m, the relative differences are 2.5% and 0.1% between the measurement and calculation. The water surface calculation compared well with the measured ones with an averaged difference of 2%. The highest difference appears at $t = 0.083$ s at 18%. The rest have a difference within 10% from the measurement. Therefore, the comparison is reasonable for these cases.

The calculated and measured peak pressure H_{PK} has a delay in Figure 2(a) of 0.012 s. This is because the water surface was extracted from the video, which gives the time an inherent uncertainty of 0.008 s at 120 fps. Additionally, the oscillation pattern after the impingement is mainly caused by the expansion and compression of the air pocket below the water column (Qian *et al.* 2020). In our model, the governing equation involved at this stage

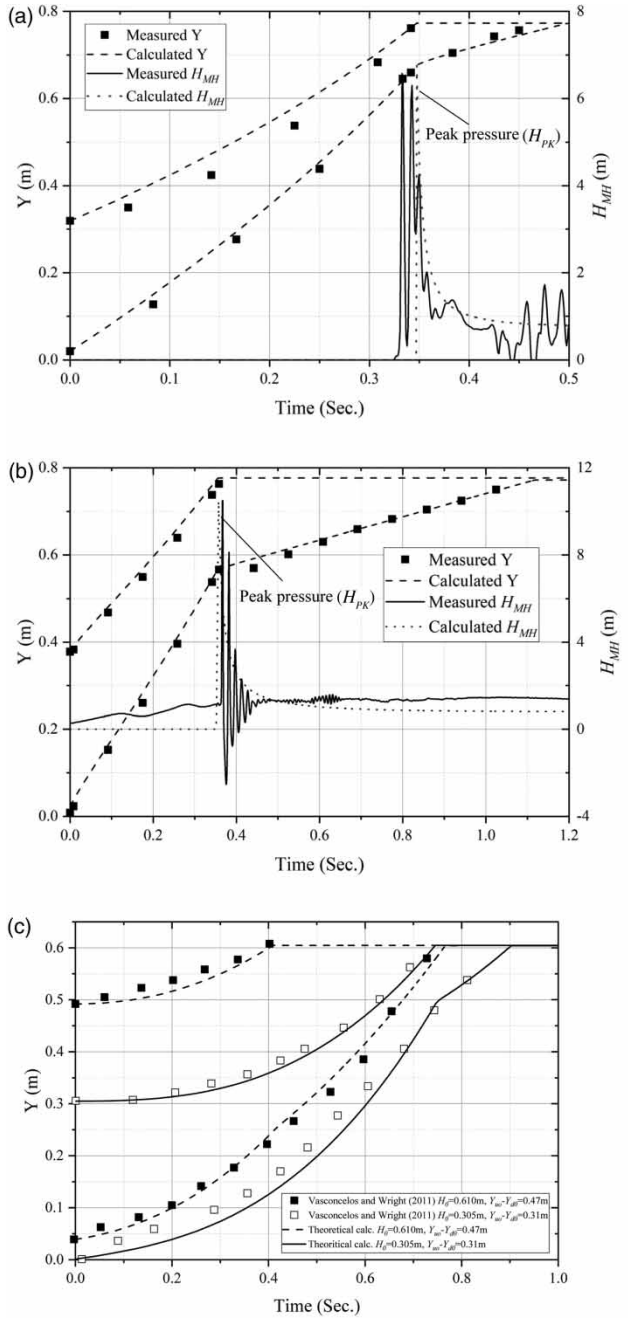

Figure 2 | Comparison between theoretical calculated and physical measurement. (a): Run A, $d/D_r = 0.5$, $\forall_0 = 71$ L, $H_0 = 1.0$ m; (b) Run A, $d/D_r = 0.1$, $\forall_0 = 71$ L, $H_0 = 1.0$ m; (c): Run B, model validation with Vasconcelos & Wright (2011) for Run B, $\forall_0 = 3.8$ L, $H_0 = 0.610$ m, $Y_{uo} - Y_{do} = 0.47$ m; and $H_0 = 0.305$ m, $Y_{uo} - Y_{do} = 0.31$ m.

(Stage 3) is Equation (15) which does not take the air phase into consideration.

Figure 2(c) shows the results of Run B based on Vasconcelos & Wright (2011). The figure shows that the calculated movement of the water column matches well with

the measurement. For Figure 2(c), the average difference between the measurement and calculation is 2% and 11% respectively for $H_0 = 0.610$ m and $H_0 = 0.305$ m. Unfortunately, there is no pressure measurement at the riser top in Vasconcelos & Wright (2011). Therefore, no pressure comparison is possible for these cases.

For all validation cases for water column movement, the root mean standard error (RMSE) between the measurement and calculation is 0.053 m. Considering the length of the riser of about 1.2 m, the RMSE is only about 1% of the length scale of the model. With a difference of 2.5% between predicted and measured pressure, the model is considered valid for further analysis.

RESULTS AND DISCUSSION

Effect of driving pressure and initial water column length

Figure 3(a) shows the relationship between the peak pressure (H_{PK}) due to water-hammer effect and the orifice opening size for Run A. The pressure firstly increases with the orifice opening size and then decreases. This trend is in agreement with Zhou *et al.* (2002) and Li & Zhu (2018). It also shows that when the driving pressure increases, the calculated H_{PK} increases. For driving pressure of 10 m, the maximum peak pressure can reach up to 53 m which corresponds to $H_{PK}/H_0 = 5.3$. For driving pressure of 5 m, the maximum peak pressure is 36 m ($H_{PK}/H_0 = 7.2$). Doubling the driving pressure from 5 to 10 m would generate an increase in the maximum peak pressure from 36 to 53 m, which is an increase of 47%. The reason for the 1.47 times increase in the maximum peak pressure for a doubling of the driving pressure is that the air below the water column acts as a cushion and damps the pressure. The reported maximum H_{PK}/H_0 is up to 40 (Li & Zhu 2018) and 15 (Zhou *et al.* 2002). In these two studies, the driving pressure pushes the water column directly, and the length of the water column increases. With an increased water mass, the momentum change is higher when the water column reaches the orifice plate, and therefore a higher peak pressure is expected.

The peak pressure is directly related to the velocity and mass of the water column when reaching the orifice plate. For a given initial water column length, a higher driving pressure generates a higher acceleration and therefore a higher velocity when reaching the orifice plate. Also, the water mass loss due to the film flow is decreased because of the shorter time taken for the water column reaching the orifice plate. Therefore, a higher driving pressure will generate a higher peak pressure for a given water column.

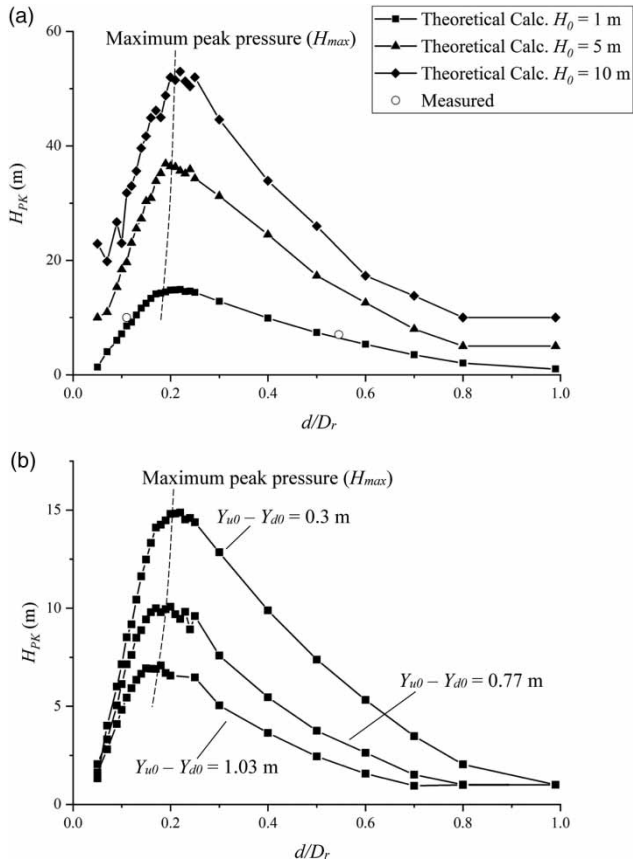

Figure 3 | Calculated peak pressure with the variation of orifice opening size for PVC risers, $\forall_0 = 71$ L, $D_r = 0.055$ m, $L = 0.78$ m. (a): With different initial pressure head at $(Y_{u0} - Y_{d0})/L = 0.39$. (b): With different initial water column length at $H_0 = 1$ m.

Figure 3(b) shows the trend of the peak pressure with different initial water column length. The figure suggests that a longer initial water column length corresponds to a smaller peak pressure. This is mainly because for a longer water column, the $(Y_u - Y_d)$ term in Equations (6) and (11) increases, and induces a lower V_u and V_d. A smaller water-hammer pressure is therefore generated. The main difference between Zhou *et al.* (2002) and the current model is that the water column is directly driven by a constant pressure in Zhou *et al.* (2002). In the current model, the water column is driven by the air pocket with initial volume of 71 L below the water column. Comparing with the results of $(Y_{u0} - Y_{d0}) = 0.3$ m and 0.77 m, an approximately 2 times the increase in the initial water column length would generate a decrease in the H_{PK}/H_0 by 30% from 15 to 10.

Effect of riser diameter and height

Run C and Run D are used to test the effect of riser diameter and height on the peak pressure. A set of representative result is plotted in Figure 4 for $(Y_{u0} - Y_{d0})/L = 0.3$, and $H_0 = 1$ m. Figure 4(a) shows the pressure variation with different riser diameters. The figure shows that for the same initial condition, a larger riser diameter corresponds to a slightly lower pressure. This is mainly because for a larger D_r, the increased riser area results in a decrease in the momentum term in Equation (8). The peak pressure induced by the water-hammer effect mainly depends on the velocity of the top of the water column. For a given initial water column length, a lower velocity gradient results in a lower velocity at the top of the water column. Therefore, a riser with a larger diameter would result in a lower peak pressure for a given initial condition.

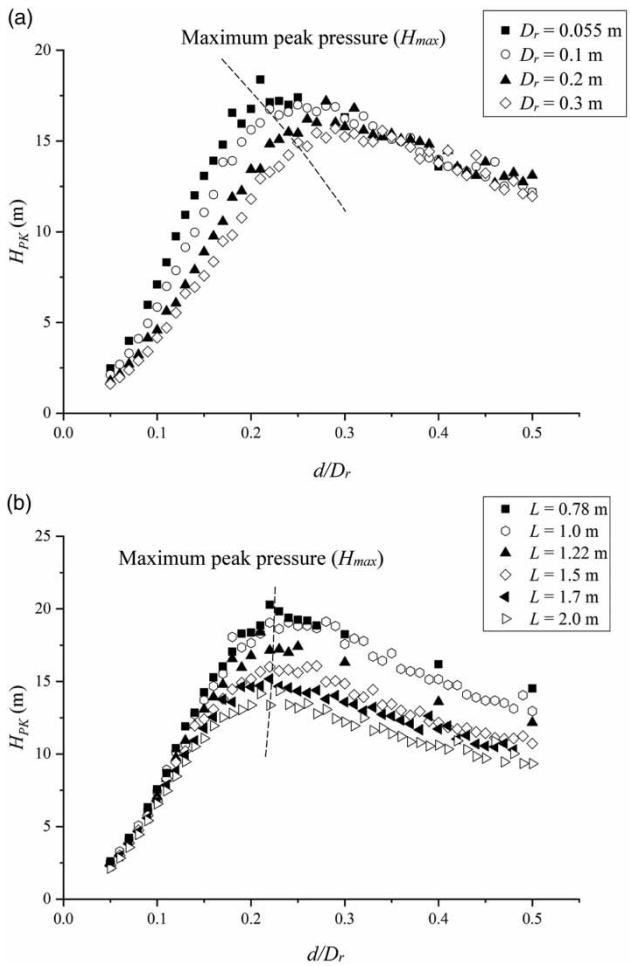

Figure 4 | Calculated peak pressure with the variation of orifice opening size for PVC risers, $\forall_0 = 100$ L, $H_0 = 1$ m, $(Y_{u0} - Y_{d0})/L = 0.3$. (a): With different riser diameter, $L = 1.22$ m; (b): With different riser height, $D_r = 0.055$ m.

From Figure 4(a), the change of peak pressure is more sensitive to the riser diameter before the peak pressure reaches the maximum. After around $d/D_r = 0.2$, the peak pressure becomes less sensitive to the riser diameter. The maximum peak pressure decreases by 13% from 17 to 15 m for riser diameter increasing by 2.56 times from 0.055 to 0.3 m. The highest standard deviation of the maximum peak pressure is 15% of the mean.

Figure 4(b) shows the simulated peak pressure for different riser height. For the same initial condition, higher riser height L corresponds to a lower peak pressure. This is mainly because for a higher riser, the initial water column length is longer for $(Y_{u0} - Y_{d0})/L = 0.3$. For a given driving pressure, a longer water column accelerates more slowly and therefore results in a lower velocity when reaching the orifice plate, inducing a lower water-hammer pressure. The change of the maximum peak pressure decreases by 21% from 19 to 15 m for riser height increasing by 2.56 times from 0.78 to 2 m. Considering the maximum peak pressure variation of 47% and 30% for doubling driving pressure and initial water column length, the maximum peak pressure is in general not sensitive to the riser diameter and height.

The maximum peak pressure in Figures 3 and 4 is denoted as H_{max}. Figure 5 is a plot of the calculated H_{max} for Runs A, C and D. The relationship between the maximum peak pressure and the ratio of the initial water column length and the initial pressure head can be written as:

$$H_{max} = 6.10[(Y_{u0} - Y_{d0})/H_0]^{-0.7} \quad (17)$$

with $R^2 = 0.94$, the coefficient 6.10, and -0.7 mainly depends on the pipe material. The figure suggests that a lower $(Y_{u0} - Y_{d0})/H_0$ corresponds to a higher H_{max}. It is

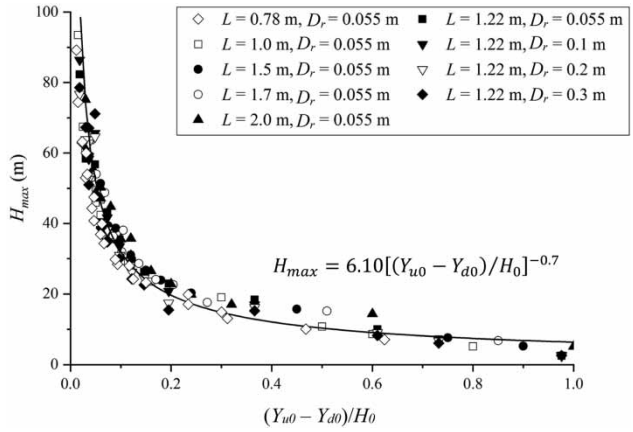

Figure 5 | Theoretical calculated maximum peak pressure for PVC riser.

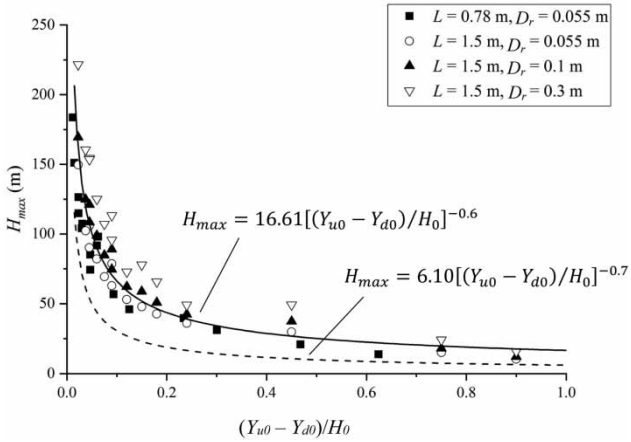

Figure 6 | Theoretical calculated maximum peak pressure for steel riser. $\forall_0 = 50$ L.

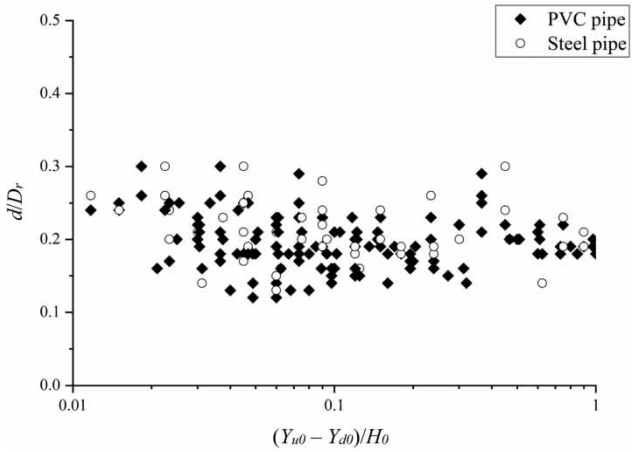

Figure 7 | Theoretical calculated orifice size when the maximum peak pressure occurs.

either due to a lower initial water column length or a higher driving pressure.

Effect of riser materials

Run E is for testing the maximum peak pressure (H_{max}) in steel pipes. Because the elastic modulus of steel pipe is higher than that of the PVC pipes, the predicted maximum peak pressure is expected to be higher than for the previous runs. Figure 6 shows the calculated maximum peak pressure for steel pipes. The maximum pressure can be fitted into:

$$H_{max} = 16.61[(Y_{u0} - Y_{d0})/H_0]^{-0.6} \quad (18)$$

with $R^2 = 0.88$; a higher coefficient at the right-hand side suggests a higher H_{max} value for a given initial condition comparing with the one of PVC pipe.

The acoustic wave speed of water in in pipes differs with the pipe material. Equation (14) suggests that for the same boundary condition, the ratio of the water-hammer type of pressure between steel and PVC riser is the ratio of the acoustic wave speed of water in these two pipes, which ranges from 1.98 to 3.62 for the tested cases (i.e. $D_r =$ 0.055 to 0.3 m). The ratio of Equations (18) and (17) yields $2.72[(Y_{u0} - Y_{d0})/H_0]^{0.1}$. The ratio ranges from 2.01 to 2.72 when the $(Y_{fs0} - Y_{int0})/H_0$ changes from 0.05 to 1, which is in the range of the theoretical range analyzed above. Therefore, the analysis above is reasonable.

Orifice opening size on maximum peak pressure

Figure 7 shows the orifice opening size when the maximum peak pressure occurs. The figure suggests that the maximum peak pressure happens when the $d/D_r = 0.13$–0.3. Among the simulated 193 cases, no obvious trend was observed. The averaged orifice size d/D_r for maximum peak pressure is 0.201 with standard deviation of 0.038. The standard deviation is 19% of the mean. Therefore, when designing orifice plates to mitigate geyser event, an orifice plate size between 0.13 and 0.3 times the riser diameter should be avoided.

CONCLUDING COMMENTS

A model was developed and numerically solved for simulating the dynamics of the geyser event with an orifice plate as a mitigation method. The proposed model focused on predicting the pressure transient when the water column in the riser is pushed by a trapped air pocket from the bottom and impinges on the orifice plate. The model was also used to assess the sensitivities between the peak pressure on the orifice plate and a variety of physical parameters.

Firstly, the sensitivity analysis suggests that the initial water column length and the driving pressure are the dominant factors for the maximum peak pressure on the orifice plate. The diameter and height of the riser have minor effects on the maximum peak pressure. Secondly, the orifice size when the maximum peak pressure occurs is between 0.13 and 0.3 times the riser diameter. When designing the orifice plate, this range should be avoided to prevent the structure from damage due to the water-hammer effect. Thirdly, a pipe with higher elastic modulus corresponds to a higher maximum peak pressure given the same initial conditions. The higher maximum peak pressure is mainly induced by the increased acoustic speed of water in pipes with different materials.

The proposed model is with a number of assumptions and therefore has some limitations. Firstly, this is a one-dimensional model where all variables vary only with time. Secondly, the model assumes pure water in the water column. For riser with a larger diameter such as in prototype systems, the formation of air/water mixture may alter the density and acoustic velocity of the water column, and therefore the parameters used in the model should be adjusted accordingly. Thirdly, this study is a laboratory scaled model and the scale effect of air/water mixture flow is still unclear. At this stage, the model is developed under ideal condition and the detailed scale effect should still be further studied to expand the current model to prototype scale.

ACKNOWLEDGEMENT

The writers gratefully acknowledge the financial support from the Natural Sciences and Engineering Research Council (NSERC) of Canada, EPCOR Inc., and Key Research and Development Program of Zhejiang (2020C03082).

REFERENCES

Arai, K. & Yamamoto, K. 2003 Transient analysis of mixed free-surface-pressurized flows with modified slot model. Part1: computational model and experiment. In: *Proceedings of ASME FEDSM'03, 4th ASME_JSME Joint Fluid Engineering Conference*, July 6–10, Honolulu, Hawaii, USA.

Beg, M. N. Z., Carvalho, R. F. & Leandro, J. 2019 Effect of manhole molds and inlet alignment on the hydraulics of circular manhole at changing surcharge. *Urban Water Journal* **16** (1), 33–44.

Chan, S., Cong, N., and Lee, J. & W, J. H. 2018 3D numerical modeling of geyser formation by release of entrapped air from horizontal pipe into vertical shaft. *Journal of Hydraulic Engineering*. doi:10.1061/(ASCE)HY.1943-7900.0001416.

City of Edmonton 2015 *Design and Construction Standards, Volume 3, Drainage*. Available from: https://www.edmonton.ca/city_government/documents/Volume_3_Drainage_.pdf.

Cong, J., Chan, S. N. & Lee, J. H. W. 2017 Geyser formation by release of entrapped air from horizontal pipe into vertical shaft. *Journal of Hydraulic Engineering*. doi:10.1061/(ASCE)HY.1943-7900.0001332.

Hamam, M. A. & McCorquodale, J. A. 1982 Transient conditions in the transition from gravity to surcharged sewer flow. *Canadian Journal of Civil Engineering* **9**, 189–196.

Huang, B., Wu, S. Q., Zhu, D. Z. & Schulz, H. E. 2018a Experimental study of geysers through a vent pipe connected to flowing sewers. *Water Science and Technology* **2017** (1), 66–76.

Huang, B., Wu, S. Q., Zhu, D. Z. & Wang, F. F. 2018b Mitigating peak pressure of storm geysering by orifice plates installed at the top of vent pipes. *Water Science and Technology* **78** (7), 1587–1596.

Lewis, J. M. 2011 *A Physical Investigation of Air/Water Interactions Leading to Geyser Events in Rapid Filling Pipelines*. PhD thesis, University of Michigan, Ann Arbor, Michigan, USA.

Li, J. & McCorquodale, J. A. 1999 Modelling mixed flow in storm sewers. *Journal of Hydraulic Engineering* **125** (11), 1170–1180.

Li, L. & Zhu, D. 2018 Modulation of the transient pressure by air pocket in a horizontal pipe with an end orifice. *Water Science and Technology* **77** (10), 2528–2536.

Liu, L. 2018 *Experimental Study on Edmonton's Storm Geyser Formation Mechanism and Mitigation Measures*. MSc thesis, University of Alberta, Edmonton, Alberta.

Liu, L., Shao, W. & Zhu, D. 2020 Experimental study on storm geyser in a vertical shaft above a junction chamber. *Journal of Hydraulic Engineering* **146** (2), 04019055.

Lopes, P., Leandro, J., Carvalho, R. F., Pascoa, P. & Martins, R. 2015 Numerical and experimental investigation of a gully under surcharge conditions. *Urban Water Journal* **12** (6), 468–476.

Potter, M. C., Wiggert, D. C. & Ramadan, B. H. 2012 *Mechanics of Fluids*, 4th edn. Cengage Learning, Stamford.

Qian, Y., Zhu, D., Liu, L., Shao, W., Edwini-Bonsu, S. & Zhou, F. 2020 Numerical and experimental study on mitigation of storm geysers in Edmonton, Alberta, Canada. *Journal of Hydraulic Engineering* **146** (3), 04019069.

Rubinato, M., Lee, S. & Martins, R. 2018 Surface to sewer flow exchange through circular inlets during urban flood conditions. *Journal of Hydroinformatics* **20** (3), 564–576.

Shao, Z. S. 2013 *Two-dimensional Hydrodynamic Modelling of two-Phase Flow for Understanding Geyser Phenomena in Urban Storm Water System*. PhD thesis, University of Kentucky, Lexington, Kentucky, USA.

Shao, Z. S. & Yost, S. A. 2018 Numerical investigation of driving forces in a geyser event using a dynamic multi-phase Navier-Stokes model. *Engineering Applications of Computational Fluid Mechanics* **12** (1), 493–505.

Vasconcelos, J. G. & Wright, S. J. 2009 Investigation of rapid filling of poorly ventilated stormwater storage tunnels. *Journal of Hydraulic Research* **47** (5), 547–558.

Vasconcelos, J. G. & Wright, S. J. 2011 Geysering generated by large air pockets released through water-filled ventilation shafts. *Journal of Hydraulic Engineering* **137** (5), 543–555.

Wright, S. J., Vasconcelos, J. G., Creech, C. T. & Lewis, J. W. 2008 Flow regime transition mechanisms in rapidly filling stormwater storage tunnels. *Environmental Fluid Mechanics* **8** (5), 605–616.

Wright, S. J., Lewis, J. W. & Vasconcelos, J. G. 2011a Geysering in rapidly filling storm-water tunnels. *Journal of Hydraulic Engineering* **137** (1), 112–115.

Wright, S. J., Lewis, J. W. & Vasconcelos, J. G. 2011b Physical processes resulting in geysers in rapidly filling storm-water tunnels. *Journal of Irrigation and Drainage Engineering* **137** (3), 192–202.

Zhou, F., Hicks, F. E. & Steffler, P. M. 2002 Transient flow in a rapidly filling horizontal pipe containing trapped air. *Journal of Hydraulic Engineering* **128** (6), 625–634.

Zhou, F., Hicks, F. E. & Steffler, P. 2004 Analysis of effects of air pocket on hydraulic failure of urban drainage infrastructure. *Canadian Journal of Civil Engineering* **31**, 86–94.

Zhou, L., Liu, D. & Ou, C. 2011 Simulation of flow transients in a water filling pipe containing entrapped air pocket with VOF model. *Engineering Applications of Computational Fluid Mechanics* **5** (1), 127–140.

First received 16 November 2019; accepted in revised form 7 April 2020. Available online 24 April 2020